Energy-Harvesting Mechanisms for UAV Flight by Dynamic Soaring

V. Bonnin, E. Benard and J.-M. Moschetta
Institut Supérieur de l'Aéronautique et de l'Espace, Toulouse, 31400 France

C. A. Toomer
University of the West of England, Bristol, England BS16 1QY, United Kingdom

ABSTRACT

Dynamic Soaring is a flying technique which extracts energy from an environment where wind gradients form, with the potential to increase the endurance of small unmanned vehicles. The feasibility to use dynamic soaring flight is questioned here; it requires the identification of energy-extraction mechanisms as well as accurate understanding of the way energy-harvesting performances are governed by trajectory constraints, vehicle characteristics and environment conditions. A three-dimensional energy-neutral trajectory is derived out of a specified optimization problem. Characteristic phases of flight are evidenced out of an overall closed trajectory. Simplified equations are used to evidence the physics behind energy transfers. Finally, overall energy-harvesting balance is studied through local variations of total energy along the path.

1. NOMENCLATURE

χ	=	position along the east direction, m
y	=	position along the north direction, m
z	=	height, m
V_i	=	inertial speed, m/s
γ_i	=	inertial flight path angle, rad
ψ_i	=	inertial azimuth angle, rad
C_L	=	lift coefficient
ϕ	=	bank angle, rad
C_{Di}	=	ith drag polynomial coefficient
b	=	span, m
S	=	wing area, m^2
ρ	=	air density, kg/m^3
g	=	gravitational acceleration, m/s^2
L	=	lift, N
D	=	drag, N
m	=	vehicle mass, kg
E_{tot}	=	total energy, earth related, J
V_{air}	=	airspeed, m/s
t_f	=	final time, s
d_t	=	time step, s
γ_{air}	=	air-relative flight path angle, rad
ψ_{air}	=	air-relative azimuth path angle, rad
C_{Lmax}	=	maximum lift coefficient
N_t	=	number of time discretization nodes
W_i	=	wind component along direction i, m/s
u^*	=	wind friction velocity, m/s
h_R	=	wind reference height, m
z_0	=	surface roughness length, m
z_{tip}	=	wing tip clearance, m

2. INTRODUCTION

2.1 Long Endurance UAV flight

Long-endurance flight is acknowledged to be a key factor of UAV utility [1]. Without any human beings on board, endurance is only limited by fuel capacity. However, in the domain of small-sized UAVs, the limited mass and volume challenge the energy storage. Besides, the smaller size comes with reduced aerodynamic efficiency by flying at lower Reynolds number and the scaling effect does not play in favour of long endurance. Innovative solutions are therefore approached in order to enable longer range and autonomy for small-sized UAVs.

Research on fuel-cell propulsion for long endurance UAV is particularly active as their high energy density potential enables to outclass hydrocarbon or electric-powered systems. Recently, the *Ion Tiger* performed a flight of 48h using only 500g of liquefied hydrogen to feed its fuel-cell [2]. However, although fuel-cells provide high specific energy together with high power, their size and volume can only be constrained to a limited level. On *Ion Tiger*, the fuel-cell system only (fuel cell, fuel tank, regulator, cooling) weights 5.5 kg [3] with neither fuel nor propulsion system. Moreover, the need for

heat transfer area increases the size of the fuselage. In order to achieve a maximum lift over drag ratio of 17, Ion Tiger has a wingspan of up to 5.15 meters, for a practical payload of 2.3 kg and an overall mass of 16 kg.

Another option for improving endurance is to seek for energy from the surrounding environment. Studies about long endurance vehicles have mainly focused on using solar power to maintain a vehicle aloft all round the clock, with the shortage of solar exposition during the night being balanced by the excess of power received throughout daylight and stored into potential energy. The *Qinetiq Zephyr* paved the way by performing a two-week-long flight in 2010 and the *Boeing Solar Eagle* project aims at staying aloft for up to five years at altitudes above 60,000 ft. Another approach is static soaring, where energy is gained by flying through a mass of rising air, either due to pockets of warm air or to wind-slope deflections. It requires detecting sparsely distributed zones of rising air and adopting an appropriate trajectory management. Several studies investigated autonomous thermal soaring for UAV and were faced with the challenge of flying through the constrained volume of thermals.

2.2 The Albatross Legacy

The technique this paper is going to focus on is called dynamic soaring. It consists in extracting energy from the wind, in an environment where vertical gradients of horizontal wind are formed. This flying technique is directly inspired by the flight of albatrosses. Those singularly massive seabirds take advantage of wind gradients which forms at the interaction between air and sea to fly for thousands of kilometres with hardly a flap of their wing [4, 5]. Since the first observations of albatrosses by Lord Rayleigh in the late XIXth century [6], the enthusiasm for dynamic soaring has grown bigger [7, 8].

Figure 1. Wandering Albatross (*Diomedea Exulans*) brushing the surface with wingtips. Copyright Klaus Berre kbphoto.dk.

Little was known about their flight until impressive travel performances were revealed by a satellite-tracking experience conducted in 1990 which showed that tagged specimens could travel more than 800 kilometres a day [9].

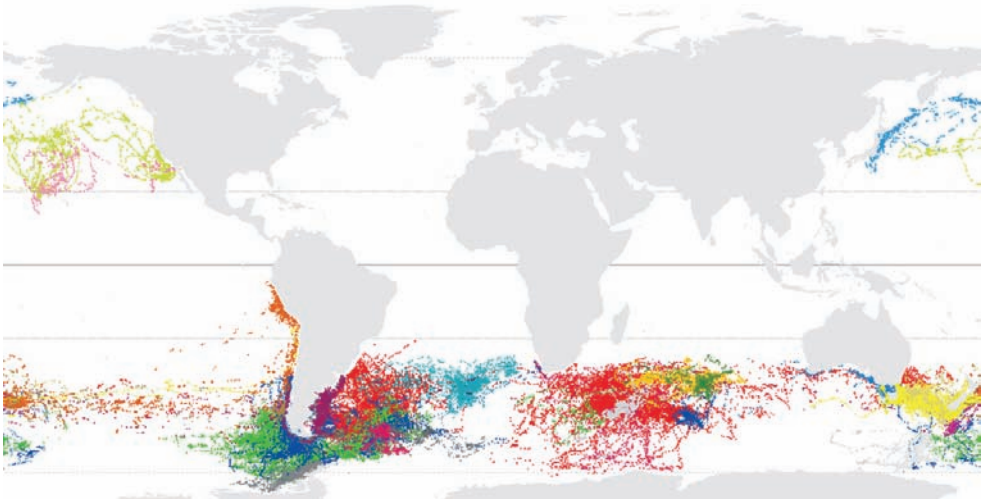

Figure 2. Satellite tracking locations of albatrosses and petrels, from [10]. All coloured-locations represent albatross species, the Wandering Albatross is shown in bright red.

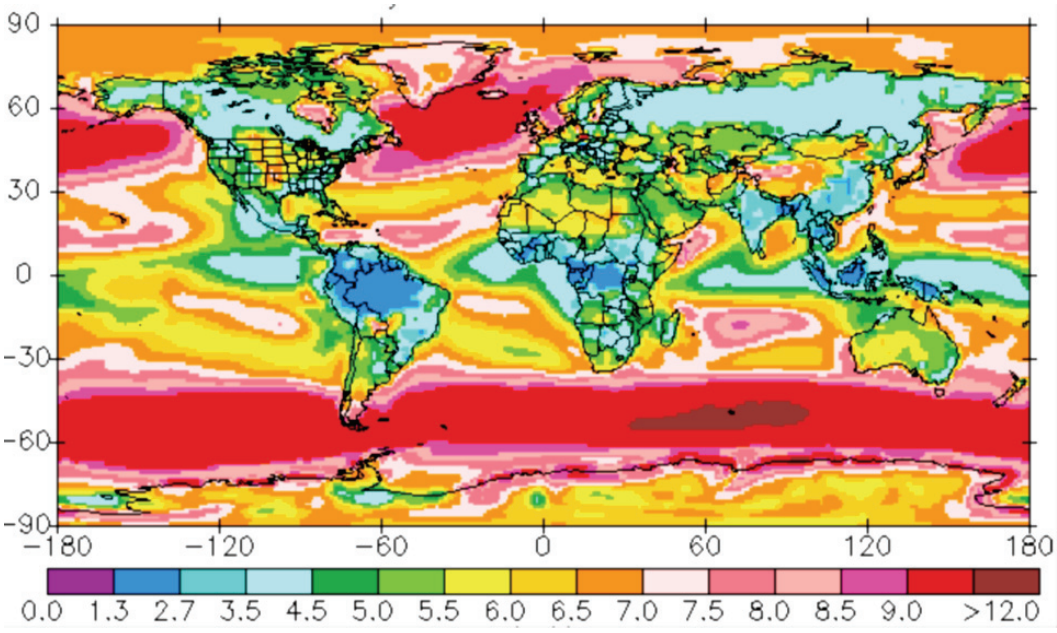

Figure 3. Estimate of wind velocity (m.s-1) at 50m, average over a 10-year period [11].

Albatross geographical distribution in Fig.2 shows a widespread presence, although rather limited to southern oceans, especially for great albatrosses of the gender *Diomedea*, like the Wandering Albatross, *Diomedea Exulans*, which can weigh up to 13kg. Many albatross species are actually endemic to a specific island and they anyway have very sparse colonies, secluded on remote islands such as Crozet, Amsterdam or Kerguelen. Their wide distribution is therefore the result of singular travel abilities which carries them all over southern oceans. However their presence is strictly out of tropical regions, with the only exception being the *Chatam Albatross* seen in orange on Fig.1. This first analysis has to be completed by a study at Fig. 3 which shows the annual estimate of global wind strength.

The correlation between wind strength and albatross presence is significant, with albatross species being reported in every zone of average wind velocity above 9 $m.s^{-1}$, except North Atlantic, and reciprocally very little albatross presence outside of those areas. Although the wind strength can not explain in itself the distribution of albatrosses around the globe, it highlights the assertion that

albatrosses use a wind-related phenomenon to propel themselves effortlessly around the globe. It should also be mentioned that the *North Pacific Albatross* species, which range from US west coast to Japan east coast, are among the lightest albatrosses, with a weight not exceeding 4.5 kg [4], while the *Great Albatross* species, including *Wandering Albatross*, are the heaviest and do not venture outside of areas of average wind velocity of 9 $m.s^{-1}$and above.

All observations of inflight albatrosses mention very little wing-flapping and biological analysis of their morphology concluded that they were not adapted to flapping flight, with long high-aspect-ratio wings and thin flight muscles [5]. The peculiarity of albatross flight technique hence does not rest upon a particular kinematic of their wings but upon specific trajectories of a fixed-wing vehicle, that are therefore potentially transposable to the domain of small fixed-wings-UAVs.

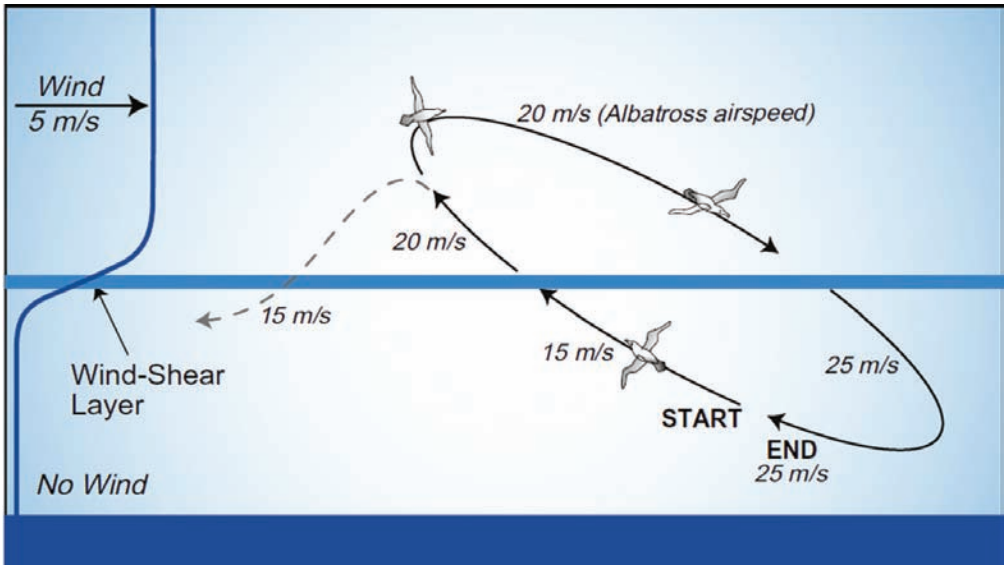

Figure 4. Overall dynamic soaring pattern and principles, from [17]. The wind profile given in the figure is not realistic but just depicts the significance of the zone of wind shear.

The basic idea behind this soaring technique is to cross layers at different windspeeds in a well-defined way, such that the manoeuvres entail a local increase in airspeed for the vehicle [6]. This cyclic pattern is simplified on Fig.4, with the albatross crossing a shear region in a repetitive motion. Albatross have in this way been observed to perform repetitive patterns, although of more intricate variations, in the first 15-20m above the surface. Several numerical studies focused on building a model of dynamic soaring applied to UAV flight [12-14]. However, the nature of energy-harvesting mechanisms has been controversial and still suffers from a lack of consistency. Pennycuick uses his observations on the field to demonstrate that albatrosses gain their energy out of gusts created by flow separation over waves [17]. Sachs and Deittert showed through numerical studies that classic wind-shear soaring over a flat ocean surface can provide conditions for sustainable dynamic soaring flight. Deittert provides a methodology that uses differential flatness, and computes trajectories for a 3m-wingspan vehicle which lift over drag ratio is evaluated at 33.4, seem rather high for a vehicle of that size. Sachs then highlighted that the energy gain comes from the upper turn from windward to leeward and he made use of albatross in-flight measurements to support his claim [16]. Richardson describes how the different energy-extraction theories are not mutually exclusive but could rather be combined during dynamic soaring flight, although no further analysis supports this claim [17].

This background of studies underlines that energy-harvesting mechanisms involved in dynamic soaring are multiple and not trivial. This paper aims at providing a clear picture of the physics involved in the energy-extraction mechanisms, in the case of wind-shear soaring. Indeed, for the sake of simplicity, our numerical model would be based on the assumption of a flat surface. Moreover, this paper would also take advantage of powerful numerical resolution tools to produce flight models of dynamic soaring and to investigate which variables govern the energy-harvesting process. The first part

would expose the methodology followed to derive dynamic soaring trajectories. Then, closed trajectory results would be extrapolated, energy extraction mechanisms would be explained and their contribution to the overall energy harvesting process would be determined.

3. METHODOLOGY

3.1 Equations of Motion

Equations of motion of a point-mass model flying through a wind environment are derived in this section. Kinematics are observed from an earth-based inertial reference frame $\mathcal{R}_0$ oriented along the North and East direction as shown in Fig. 5.

The inertial speed $\mathbf{V_i}$, defined in Eq.1a, is oriented with azimuth and flight path angles with respect to $\mathcal{R}_0$, as presented in Fig. 5, defining a $\mathcal{R}_i$ reference frame so that the inertial speed is oriented along $\mathbf{x_i}$, in the same direction. The airspeed is then oriented with respect to $\mathcal{R}_0$ using also a set of azimuth and elevation angles and the lift is oriented by the bank angle ϕ, as shown in Fig. 6. Moreover the wind is supposed to be unidirectional, coming from the north only. This is introduced in Eq. 1c.

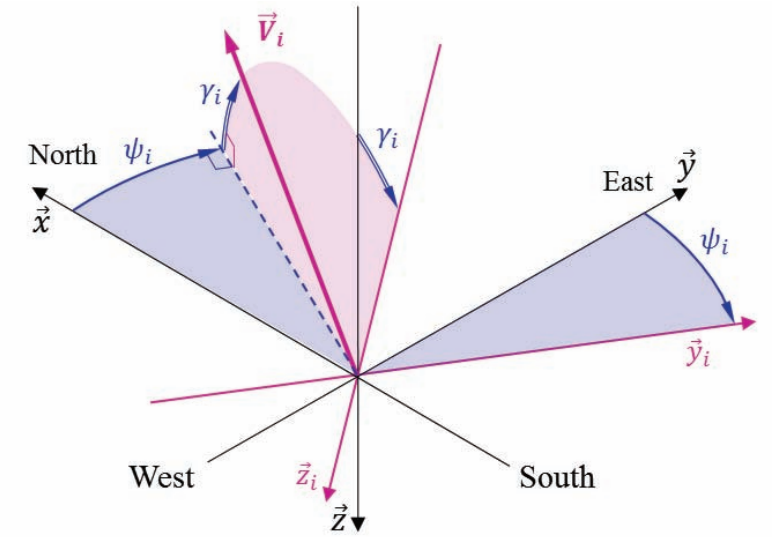

Figure 5. The orientation of the inertial speed with respect to the reference frame $\mathcal{R}_0$.

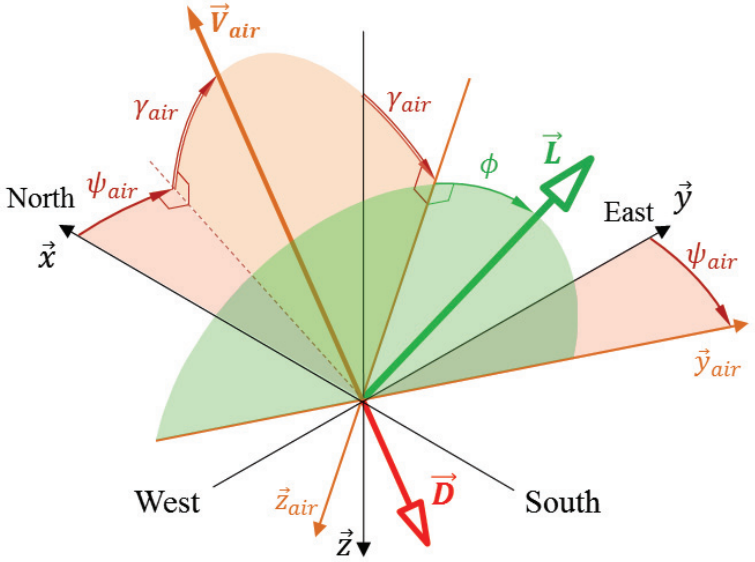

Figure 6. Orientation of the airspeed and of aerodynamic forces, with respect to the reference frame $\mathcal{R}_0$.

$$\vec{V}_i = V_i.\vec{x}_i \tag{1a}$$

$$\vec{V}_{air} = V_{air}.\vec{x}_{air} \tag{1b}$$

$$\vec{W} = -W_x.\vec{x} \tag{1c}$$

The inertial speed consists of the combination of the speed relative to the ambient air with the speed of air relative to earth. This vector expression is expressed by Eq.2, and is decomposed into Eqs 2a-2e, which specify norm and angle relations.

$$\vec{V}_{air} = \vec{V}_i - \vec{W} \tag{2}$$

$$V_{air} = \sqrt{{V_i}^2 - 2.V_i.W_x.cos\,\psi_i.cos\,\gamma_i + {W_x}^2} \tag{2a}$$

$$\sin\gamma_{air} = \frac{V_i.sin\,\gamma_i}{V_{air}} \tag{2b}$$

$$\cos\gamma_{air} = \sqrt{1 - \sin^2\gamma_{air}} \tag{2c}$$

$$sin\,\psi_{air} = \frac{V_i.cos\,\gamma_i.sin\,\psi_i}{V_{air}.cos\,\gamma_{air}} \tag{2d}$$

$$\cos\psi_{air} = \frac{V_i.cos\,\gamma_i.cos\,\psi_i - W_x}{V_{air}.\cos\gamma_{air}} \tag{2e}$$

Newton's second law rights down in Eq. 3.

$$m\,\frac{d\vec{V}_i}{dt})_{R_0} = \sum \overrightarrow{\text{Forces}}_{ext\to vehicle} \tag{3}$$

The derivation formula is applied to the inertial speed in Eqs. 3a-3c.

$$\frac{d\vec{V}_i}{dt})_{R_0} = \frac{d\vec{V}_i}{dt})_{R_i} + \vec{\Omega}_{R_i/R_0} \wedge \vec{V}_i \tag{3a}$$

$$\vec{\Omega}_{R_i/R_0} = \dot{\gamma}_i\vec{y}_i + \dot{\psi}_i\,\vec{z_i} \tag{3b}$$

$$\frac{d\vec{V}_i}{dt})_{R_0} = \dot{V}_i\ \vec{x_i} + V_i\cos\gamma\,\dot{\psi}_i\,\vec{y_i} - V_i\,\dot{\gamma}_i.\vec{z_i} \tag{3c}$$

Equations of motion are obtained by projection of Eq. 3c on $\mathcal{R}_i$. Contributions from lift, drag and weight add to form the following expressions along the ***x, y, z*** axis.

$$F_x = -L\,(sin\,\phi\,\sin\psi_{air} + cos\,\phi\,cos\,\psi_{air}\,sin\,\gamma_{air}) - D\,\cos\gamma_{air}\cos\psi_{air} \tag{4a}$$

$$F_y = L\,(sin\,\phi\,cos\,\psi_{air} - cos\,\phi\,sin\,\psi_{air}\,sin\,\gamma_{air}) - D\,cos\,\gamma_{air}\,sin\,\psi_{air} \tag{4b}$$

$$F_z = -L\ cos\,\phi\cos\gamma_{air} + D\,\cos\gamma_{air} + mg \tag{4c}$$

The first three equations of motion are therefore explicited in Eqs 5a-5c.

$$m\dot{V}_i = F_x \cos\gamma_i \cos\psi_i + F_y \cos\gamma_i \sin\psi_i - F_z \sin\gamma_i \tag{5a}$$

$$m\mathrm{V}_i \cos\gamma_i \,\dot{\psi}_i = -F_x \sin\psi_i + F_y \cos\psi_i \tag{5b}$$

$$-m\mathrm{V}_i \,\dot{\gamma}_i = F_x \sin\gamma_i \cos\psi_i + F_y \sin\gamma_i \sin\psi_i + F_z \cos\gamma_i \tag{5c}$$

The kinematic equations are given in Eqs 6a-6c and provide three other equations.

$$\dot{x} = \mathrm{V}_i \cos\gamma_i \cos\psi_i \tag{6a}$$

$$\dot{y} = \mathrm{V}_i \cos\gamma_i \sin\psi_i \tag{6b}$$

$$\dot{z} = -\mathrm{V}_i \sin\gamma_i \tag{6c}$$

Lift and drag are expressed as in Eqs. 7a-7b.

$$\mathrm{L} = {}^{1}\!/_{2}\,\rho.\mathrm{S}.C_L.{V_{air}}^2 \tag{7a}$$

$$D = {}^{1}\!/_{2}\,\rho.\mathrm{S}.\left(C_{D0} + C_{D1}.C_L + C_{D2}.{C_L}^2 + C_{D3}.{C_L}^3 + C_{D4}.{C_L}^4\right).{V_{air}}^2 \tag{7b}$$

3.2 Vehicle Model

As dynamic soaring flight is directly inspired by the flight of albatrosses, the vehicle was initially given the properties of the *Wandering Albatross* for the sake of validation. Sachs has come to an estimate about the possible characteristics of an albatross, based on measurements and data from different authors [12].This model has been used by different other authors for their numerical studies and is therefore a good support for validation. As modelled by Sachs, the albatross has a wingspan of 3.3 m and achieves a maximum lift over drag ratio of 20 at an airspeed of 13 m/s. Pennycuick uses measurements from the field and home-made aerodynamic software to compute a model of very similar dimensions, with a maximum lift over drag ratio of 21 at an airspeed of 15.5 m/s.

However, another vehicle model will be used for the remainder of this paper, based on the architecture of a small-scale glider rather than a bird, as shown in Fig.5. That will suppress the need to estimate and to average a geometry between different albatross specimens and will make sure that the performances of the model are achievable by an engineering-designed vehicle. The vehicle which is going to be considered has been developed by Bower and is optimized for dynamic soaring flight [18]. Contrary to albatross which can have a wing tip touching the water, the ability of a UAV to fly very close to the surface is limited, therefore the vehicle has a smaller wingspan of 2.5 m in order to keep the centre of gravity as close to the surface as possible during manoeuvres at low height and high bank angles. The vehicle manages to overcome this span penalty by taking advantage of a SD 7037 aerofoil to reach a maximum lift over drag ratio of 20.5. The model designed by Bower has a base mass of 2 kg, on top of which a payload of 4.6 kg is added. It is assumed that the basic design can handle the higher structural loads.

Table 1. Vehicle model parameters

Parameter	Albatross	Vehicle
m	8.5 kg	6.6 kg
b	3.3 m	2.5 m
S	0.65 m^2	0.485 m^2
AR	16.81	12.8
C_{Lmax}	1.6	1.17
$(C_L/C_D)_{max}$	20	20.5

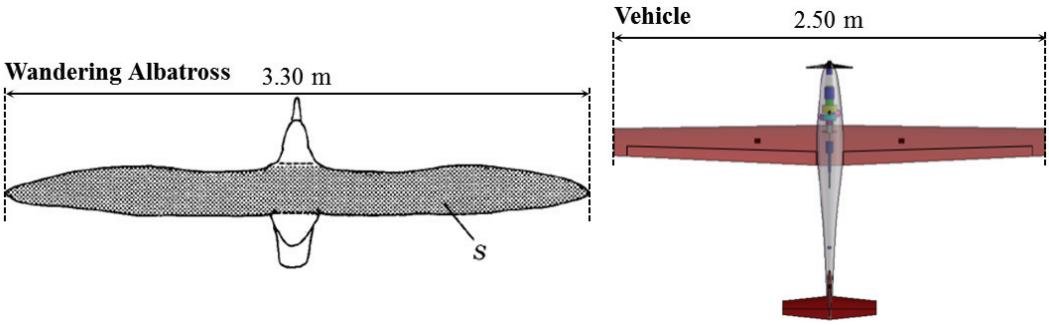

Figure 7. Comparison between a wandering albatross and the vehicle selected.[18]

3.3 Wind Model

The vertical distribution of wind shear over the ocean is an important factor to consider as it highly conditions the feasibility to sustain dynamic soaring flight. Indeed, not only the wind strength plays an important part in the energy-extraction process but so does the vertical gradient of horizontal wind, that is to say the way the horizontal wind increases with altitude. For the sake of simplicity, the surface is assumed to be rather flat. However the presence of waves is taken into account statistically by variations on the roughness length in the models. Over land, the logarithmic wind profile is used extensively to model the atmospheric boundary layer below 100 m, where the wind varies with height as expressed in Eq. 8. The *log* refers to the natural logarithm and χ is the Von Karman constant, which value is *0.41*.

$$W(z) = \frac{u_*}{\chi} \, log \, \frac{z}{z_0} \tag{8}$$

The roughness length z_0 is a function of the underlying surface characteristics; the value of z_0 depends on the size, form and spacing of surface protrusions. It ranges from a few millimeters for the open sea to the order of the meter for cities or forests. A value of 3 cm for z_0 will be chosen in the remainder of this paper for z_0, which corresponds to an open flat terrain with grass and sparse obstacles. It seems a good compromise between typical roughness lengths at sea and over land. Moreover, the wind is assumed to be steady and unidirectional, coming from the North. Therefore the wind field is defined as in Eq. 9.

$$\begin{cases} \mathrm{W}_x(\mathrm{z}) = -\dfrac{u_*}{\chi} \, log \, \dfrac{z}{z_0} \\ \mathrm{W}_y(\mathrm{z}) = 0 \\ \mathrm{W}_z(\mathrm{z}) = 0 \end{cases} \tag{9}$$

3.4 Optimization Problem

The movement of the point-mass model is described by the evolution of the six state variables through Eqs. 5a-5c and Eqs. 6a-6c. This evolution is governed by the state of the system itself and by variations of control variables, which are in this case the bank angle ϕ and the coefficient of lift C_L. An efficient way to find out the evolution of control variables that would produce a trajectory which extracts energy from the wind by dynamic soaring is to solve an optimization problem. From a basic knowledge of dynamic soaring principles that will help to set an initial guess for variables, the optimization would find the particular trajectory that maximizes or minimizes an objective function while abiding by a set of constraints.

The objective function in this case would be to minimize the wind strength that is necessary to perform dynamic soaring cycles of trajectory without any energy input from the vehicle. The wind

strength is expressed by the value u_* of the friction velocity. A set of constraints completes the problem. First of all, the cycles should be defined by a trajectory between two comparable states of the system, such that those cycles would be reproducible one after the other identically. The trajectory should therefore include periodicity requirements which should affect, if not all, some of the six state variables which define the system. Then certain operational limitations need to be taken into account, such as imposing a wing tip clearance above the water and avoiding stall. Equations of motion are taken into account as constraints and initial conditions must be specified as well as final conditions when variables are subject to periodicity. This gives the following optimization problem.

Minimize	*Friction velocity*	u_*
Subject to	*No stall*	$\mathrm{C}_L \leq 1.17$
	Max. bank angle	$-85^o \leq \phi \leq 85^o$
	Max. flight path angle	$-75^o \leq \gamma \leq 75^o$
	Wing tip clearance	$50\ cm \leq -z \pm \frac{b}{2}(cos\ \gamma_{air} \sin \phi)$
	Equations of motion	*Eqs 5a-5c, Eqs 6a-6c*
	Initial Conditions	$\{V_i^{initial}; \psi_i^{initial};\ \gamma_i^{initial}; \mathrm{x}^{initial}; y^{initial};\ \mathrm{z}^{initial}\}$
	Periodicity	$\{V_i^{initial}; \psi_i^{initial};\ \gamma_i^{initial};\ \mathrm{z}^{initial}\} = \{V_i^{final}; \psi_i^{final};\ \gamma_i^{final};\ \mathrm{z}^{final}\}$

Numerical analysis will solve this problem using collocation technique [20,21]. The infinite dimension problem is converted into a parameterized problem by discretizing the solution time history into a number of intervals, which will be of constant length *dt* here. The state variable evolution with time, stated in Eqs 5a-5c and Eqs 6a-6c, is approximated over each interval using interpolation techniques at some well-defined interpolation points, called collocation points. The equations of motion are then verified over each interval by bringing a residual to zero as part of the optimization process. Fourth-order Simpson one-third rule is used in this case with a Hermite-cubic polynomial that interpolates the evolution of control variables over each interval. Equations of motion are then satisfied at the midpoint of each interval by bringing the residual expressed in Eq. 10c to zero. The integration of equations of motion is therefore part of the optimization process. In this implicit integration scheme, the solver iterates on both state and control variables to reach an optimum. So for the vector of state variables **X**, the vector of control variables **u,** the vector function **g** representing the equations of motion, over a time interval of length *dt* between collocation points *k* and *k+1*, the state variables are evaluated as Eq. 10a and the control variables as in Eq. 10b.

$$\mathrm{X}_m = \frac{\mathrm{X}_k + \mathrm{X}_{k+1}}{2} - \frac{1}{8}.\left(g(\mathrm{X}_{k+1}, u_{k+1}) - g(\mathrm{X}_k, u_k)\right).dt \tag{10a}$$

$$\mathrm{u}_m = \frac{\mathrm{u}_k + \mathrm{u}_{k+1}}{2} \tag{10b}$$

For each state variable $\{\mathrm{X}^1, \mathrm{X}^2, ..\mathrm{X}^i, .., \mathrm{X}^6\}$,the residual is expressed as in Eq. 8c.

$$\mathrm{R}_k^i = \mathrm{X}_{k+1}^i - \mathrm{X}_k^i - \frac{1}{6}.\left(g^i(\mathrm{X}_k, u_k) + 4.g^i(\mathrm{X}_m, u_m) + g^i(\mathrm{X}_{k+1}, u_{k+1})\right).dt \tag{10c}$$

This is a nonlinear constrained optimization problem. Moreover as the residual at collocation point k is

a function of state variables at k and k+1 only, the Jacobian matrix relative to the problem is sparse. The solver SNOPT [22] is appropriate for this type of problem and was chosen to found an optimum. The Jacobian matrix is passed to the solver by pre-solving the problem with AMPL, which calculates the coefficient or gradients using finite differencing.

4. ENERGY-HARVESTING PROCESS

4.1 Closed Trajectory

One of the characteristics of dynamic soaring, as opposed to static soaring, is that the energy transfer from the wind to the vehicle occurs through dynamic manoeuvres where the energy-harvesting rate is not continuous but sees gains and losses. For this reason, energy-extraction mechanisms are difficult to understand and to model as they are bound up with other variations of kinetic and potential energy along the flight path. It is therefore necessary to study the kinematics of the vehicle in order to investigate the associated energy-extraction mechanisms.

Among different potential trajectories, the closed loop is of particular interest as the vehicle is forced to reach back its initial position, so that the initial and the final state are identical. The optimization process is run to derive a closed trajectory which minimizes the wind strength required to fly effortlessly, that is to say without any power supplied by the vehicle. In the formulation of the optimization problem, periodicity constraints are imposed for each state variable.

It may be possible that such a trajectory does not exist, whatever the wind friction velocity is, even very high. In such a case, there is no solution to the problem and dynamic soaring cannot be considered as a viable way to loiter over a fixed location. It may require some adjustments over some design variables such as the mass of the vehicle for instance, or alterations of some environment variables, such as the surface roughness length.

Therefore, this approach will question the feasibility for the vehicle to perform a closed loop within an environment of positive vertical wind shear gradient of variable strength, as well as provide a support to study variation in total energy during the cycle. It is to mention that the energy ratio between the initial state and the final state is 1, therefore the energy extracted along the path exactly compensates drag losses and the vehicle can stay aloft by repeating the exact same trajectory without the need to provide extra power.

The wind required to perform that closed loop energy-neutral trajectory will serve as a benchmark regarding the feasibility, for a vehicle, to remain effortlessly in the air over a fixed position by using dynamic soaring. If the actual wind is less that the benchmark value, then some power must be provided to conserve the level of total energy over one cycle. If the actual wind is more that the benchmark value, then the vehicle can enter the next cycle with some extra energy, therefore allowing margin for additional manoeuvres, such as travelling in one direction, before repeating the same cycle.

The trajectory shown in Fig. 8 is the result of the optimization problem explicated above. A solution exists and is obtained for w wind friction velocity of 80 cm/s, which corresponds to a wind speed of 11.34 m/s at 10 m. The optimal closed trajectory consists in an 8-shaped path rather than a simple loop.

It combines different legs which are characteristic to dynamic soaring flight. An upwind climb where the vehicle climbs straight into the wind, wings level, is followed by a turn from upwind heading to downwind heading where the maximal height is reached with a belly exposed to the wind attitude and a high bank angle, up to 80 degrees. Then starts a downwind dive, where the vehicle levels back wings and builds up inertial speed quickly. That is followed by the last maneuver, a turn into the wind at almost constant height close to the surface.

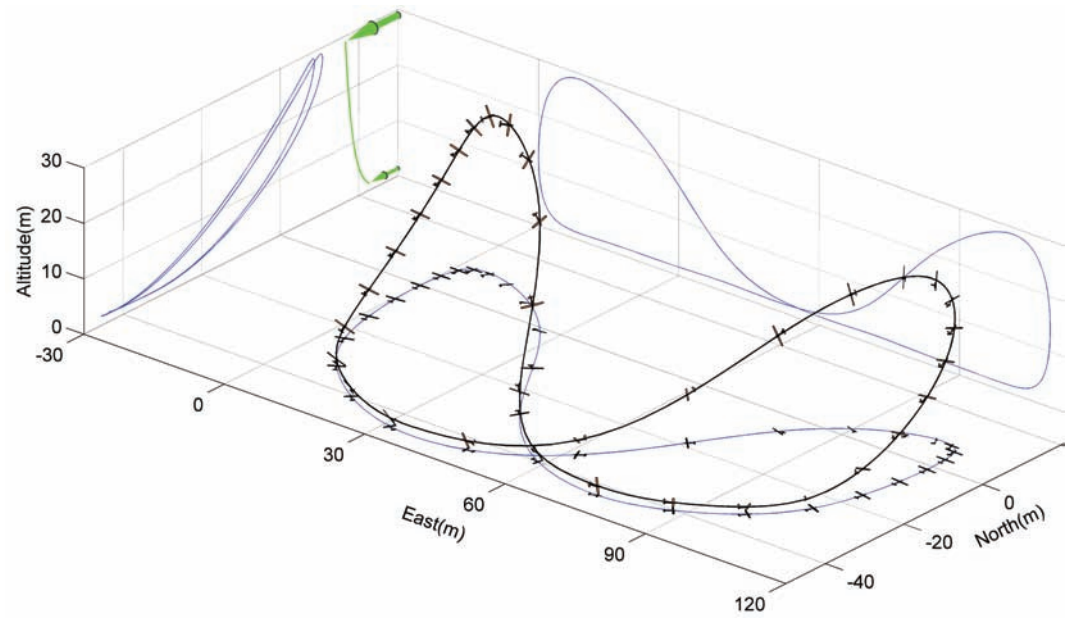

Figure 8. Closed loop energy neutral trajectory obtained for a wing tip clearance of 50 cm, a surface roughness length of 3 cm and a wind friction velocity of 80 cm/s, which corresponds to a wind speed of 11.34 m/s at 10 m. The trajectory is completed in 20.58 s. The wind profile is represented in green, between the minimum and maximum altitude

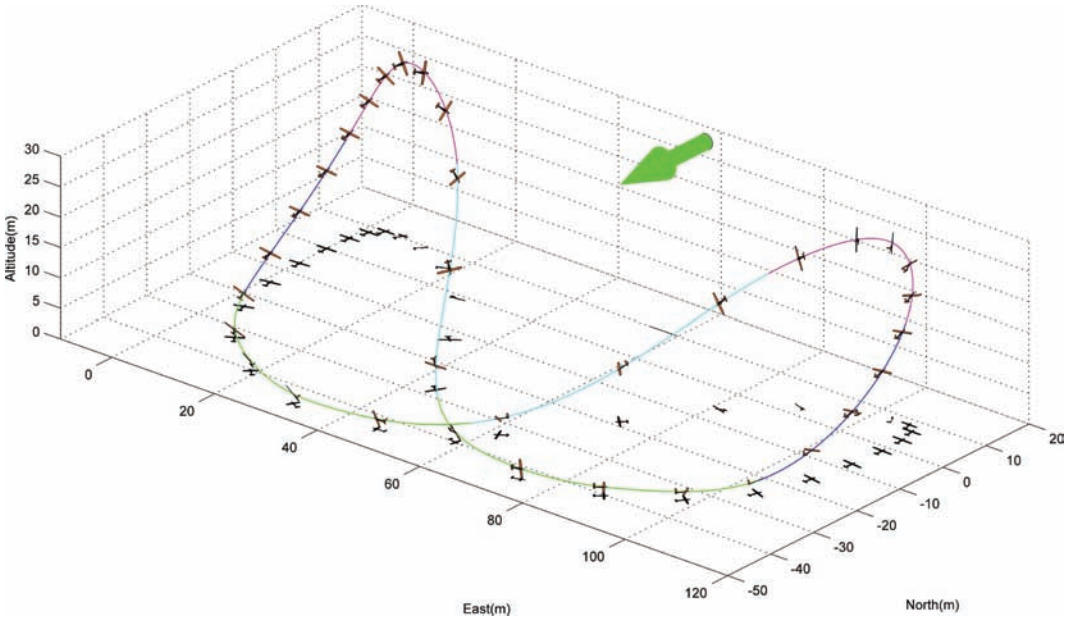

Figure 9. Phases of flight are evidenced out using different colors. Blue for the upwind climb, magenta for the high turn, cyan for the downwind dive and green for the lower turn.

The two inner loops which compose the 8-shaped path slightly differ in amplitude but are identical in their construction; therefore we can limit our scope to one loop of the overall trajectory, which consists of the four legs mentioned above.

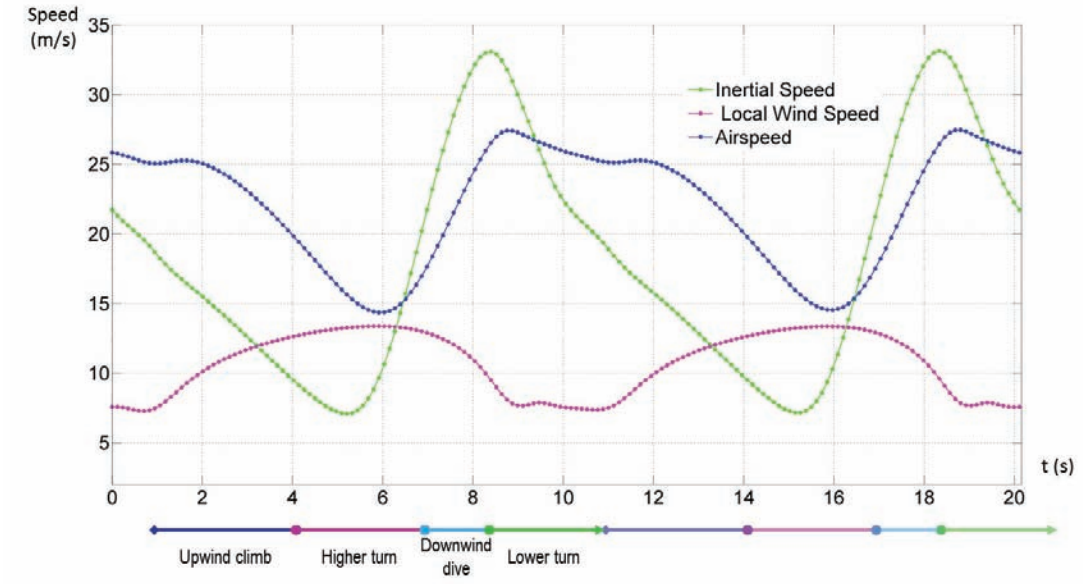

Figure 10. Speeds along the path, correlated to the four phases of flight.

Fig.10 details the variation of different speeds along the path, in order to improve the understanding of the way those are associated to the four phases of flight. The wind strength at the vehicle's altitude is also pictured and gives a direct image of the height of the vehicle.

On the upwind climb, the vehicle starts to pull up upwind and to climb through a zone where the vertical wind gradient is the strongest, since it is the lower part of the path, close to the surface. An associated local increase in airspeed can be observed, which is however not sustained for long as the wind gradient is not strong enough to allow for a steady airspeed. Besides, the rate of decrease in inertial speed gets lower as soon as the vehicle pulls up. This seems somehow counter-intuitive as the negative contribution of the weight adds up to drag losses as soon as the flight path deflects upwards, creating an even greater negative work contribution to the variation in kinetic energy. Hence, it can be deduced that another force provides a positive contribution to overcome this influence. Given that only three forces act on the vehicle, it can be deduced that the lift gives a positive work contribution during the headwind climb.

The vehicle then performs an upper turn from a windward heading to a leeward heading. The inertial speed sharply increases when the vehicle gets pulled by the wind before reaching its highest altitude of 29 m. The rate of increase in inertial speed is significantly higher than the rate of increase in airspeed, suggesting that the lift provides a positive contribution to the movement. The airspeed has a smoother variation and reaches a minimum at the top of the path, when the vehicle starts to head down.

The vehicle follows with is the leeward dive. The inertial speed keeps increasing for some time before reaching a maximum when the vehicle starts the turn against the wind. The airspeed sees the combined effects of gain in kinetic energy during the descent and of decreasing tailwind as the vehicle goes down leeward through the vertical wind shear gradient. The latter effect is strong enough to keep the airspeed increasing after the inertial speed starts to reduce. The airspeed maximum is reached when the vehicle stabilizes at a low altitude at the end of the dive.

The last component of the trajectory is the lower turn, where the vehicle turns into the wind, from leeward to windward, close to the surface at a constant height, in a zone of weak wind. The inertial speed sharply decreases at a much higher rate than the airspeed, suggesting that the lift provides a negative contribution during the lower turn.

Overall, the vehicle manages to perform a non-powered closed trajectory and to maintain its energy level between the initial and the final state. It takes advantage of a wind gradient that is not strong enough to sustain steady airspeed during the climb, which takes aback a common misbelief about dynamic soaring [15]. Indeed, it has been assumed before that the wind gradient should be strong enough to enable the airspeed to be constant during the climb, when the inertial speed decreases. This paper shows that this condition is not required. Besides, the energy neutral trajectory was achieved for

a nominal wind at ten meters of 11.34 m/s, which is the minimal wind strength that enables the energy ratio to reach 1 for this kind of closed trajectory.

4.2 Energy-Extraction Mechanisms

Dynamic soaring manages to take advantage of local contributions of aerodynamic forces along the flight path by combining specific manoeuvres with respect to the wind field. In the case of static gliding flight in still air, airspeed and inertial speeds are the same and only the drag contributes to the variation of total energy, as the lift is orthogonal to the direction of motion. However, if the vehicle flies through a mass of moving air, variations in total energy, in the earth reference frame, will see a contribution from the lift as well. It is to be noted that the work done by forces varies with the point of view of the observer. From an earth-based point of view, Fig. 11 shows how forces and speeds orientate during a windward climb. It is assumed that wings are level and that airspeed, inertial speed and wind speed are in the same plane. The orientation of the inertial speed and of the wind speed induces that the airspeed is not directed along the direction of motion, but forms an angle (γ_i - γ_{air}) with it. Aerodynamic forces are therefore also tilted with respect to the frame of reference $\mathcal{R}_i$ since the lift and the airspeed are orthogonal while the drag and the airspeed are collinear.

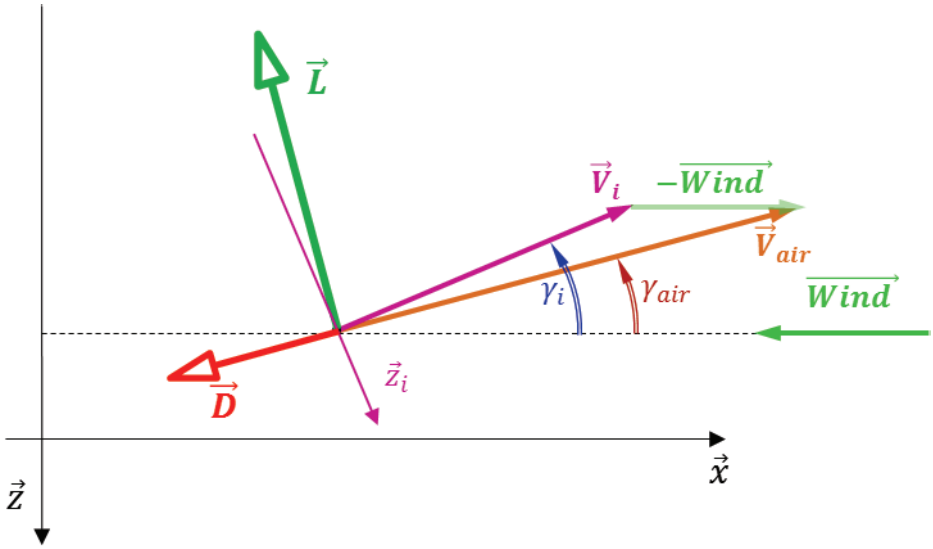

The variation of total energy is only driven by contributions of non-conservative forces, that is to say only the lift and the drag. The calculation of the elementary variation in total energy takes into account the respective work done by those forces, as shown in Eqs. 11a-11c.The elementary displacement *dl* is along the inertial direction $\mathbf{x_i}$.

$$dE_{tot} = dW_{Non\ Conservative\ Forces} = \sum_{NCF} \vec{F}.\overrightarrow{dl} = \left(\vec{L} + \vec{D}\right) \cdot (dl.\overrightarrow{x_i}) \tag{11a}$$

$$dE_{tot} = [L\ \sin(\gamma_i - \gamma_{air}) - D\ \cos(\gamma_i - \gamma_{air})]\ dl \tag{11b}$$

$$\Delta E_{tot}{}_A^B = \int_A^B [L\ \sin(\gamma_i - \gamma_{air}) - D\ \cos(\gamma_i - \gamma_{air})].\ dl \tag{11c}$$

Therefore, the condition to a local increase in total energy is expressed in Eq. 11d and Eq. 11e. Equation 11e is obtained through some calculations involving Eq. 2b and Eq. 2e.

$$dE_{tot} \geq 0 \quad if \quad \frac{L}{D} \geq \frac{1}{\tan(\gamma_i - \gamma_{air})} \tag{11d}$$

$$dE_{tot} \geq 0 \quad if \quad \frac{L}{D} \geq \frac{\left({}^{V_i}/_{-W_x}\right) + \cos\gamma_i}{\sin\gamma_i} \tag{11e}$$

Equation 11e underlines how the local energy-extraction is sensible to the instantaneous lift over drag ratio, which should be as high as possible, and for a large range of C_L since the vehicle explores a full range of functioning points during the climb. Moreover, it shows the sensitivity of the energy-extraction to both the inertial flight path angle γ_i and to the local wind strength $-W_x$. A steep climb into a strong wind would represent a favorable case for a given vehicle. It should be mentioned that for an inertial speed twice the value of the local wind and at a *30°* climb angle, the lift over drag ratio has to be over 5.7 in order to extract energy, which is easily achievable. It can be concluded that any average glider can extract energy during an upwind climb.

The rate of variation in total energy is expressed in Eq. 12a. The contribution of the lift can be simplified to the scalar product between the lift and the wind, as the lift is orthogonal to the air speed vector. The power due to lift is developed in Eq. 12.c, where components of two distinct contributions can be outlined.

$$\frac{dE_{tot}}{dt} = \sum_{NCF} \vec{F}.\vec{V_i} = \left(\vec{L} + \vec{D}\right) \cdot (V_i.\vec{x}_i) \tag{12a}$$

$$\vec{L} \cdot \vec{V_i} = \vec{L} \cdot (\vec{V_{air}} + \vec{W}) = \vec{L} \cdot \vec{W} \tag{12b}$$

$$\vec{L} \cdot \vec{W} = -\frac{1}{2}\, \rho\, S\, C_L\, {V_{air}}^2\, W_x\, (\sin\phi \sin\psi_{air} + \cos\phi \cos\psi_{air}\ \sin\gamma_{air}) \tag{12c}$$

The first corresponds to the case seen before, with wings level ($\phi = 0$). The lift works positively when either the vehicle is facing the wind ($\psi_{air} = 0$) and the vehicle is climbing ($\gamma_{air} > 0$), or when the vehicle flies leeward ($\psi_{air} = \pi$) and the vehicle is descending ($\gamma_{air} < 0°$). Consequently, not only the lift contributes positively to an increase in total energy when the vehicle is climbing into the wind, but it does also provide power to the vehicle when it is diving downwind.

The other contribution corresponds to the case where the vehicle flies crosswind in such a way that the longitudinal axis of the vehicle is orthogonal to the wind direction, if it is assumed that there is no sideslip. Considering the case where the wind comes from the left of the vehicle ($\psi_{air} = \pi/2$), it can be seen that the lift works positively when the vehicle turns right ($\phi > 0$), that is to say opposite to the wind. This corresponds to the "belly to the wind" attitude of albatrosses described by Pennycuick [15]. Inversely, if the vehicle turns left into the wind ($\phi < 0$), then the lift contributes negatively. The same applies when the wind comes from the right of the vehicle.

Those simplified calculations highlight that during a closed loop such as the one obtained in Fig. 8, the lift contributes to an increase in total energy during the upwind climb, as well as during the upper turn into the wind and also through the downwind dive. The last phase which appears during the loop is the turn into the wind, which sees inversely a negative contribution from the lift. It should be noted that those statements remains valid whatever the wind profile $W_x(z)$ is, even if the wind is uniform with no vertical gradients. However, the wind profile will determine how those respective gains and losses would weight respectively to each other in the overall energy balance.

4.3 Overall cycle of total Energy

If local manoeuvres can be performed in order to extract energy through the mechanisms that have been specified, a closed trajectory must however combine a series of those manoeuvres such that the vehicle gets back to its initial position. The set of successive manoeuvres is a delicate solution of an optimization problem that compromises the objective function in order to satisfy periodicity constraints. From that perspective, an open loop trajectory can take advantage of a greater flexibility

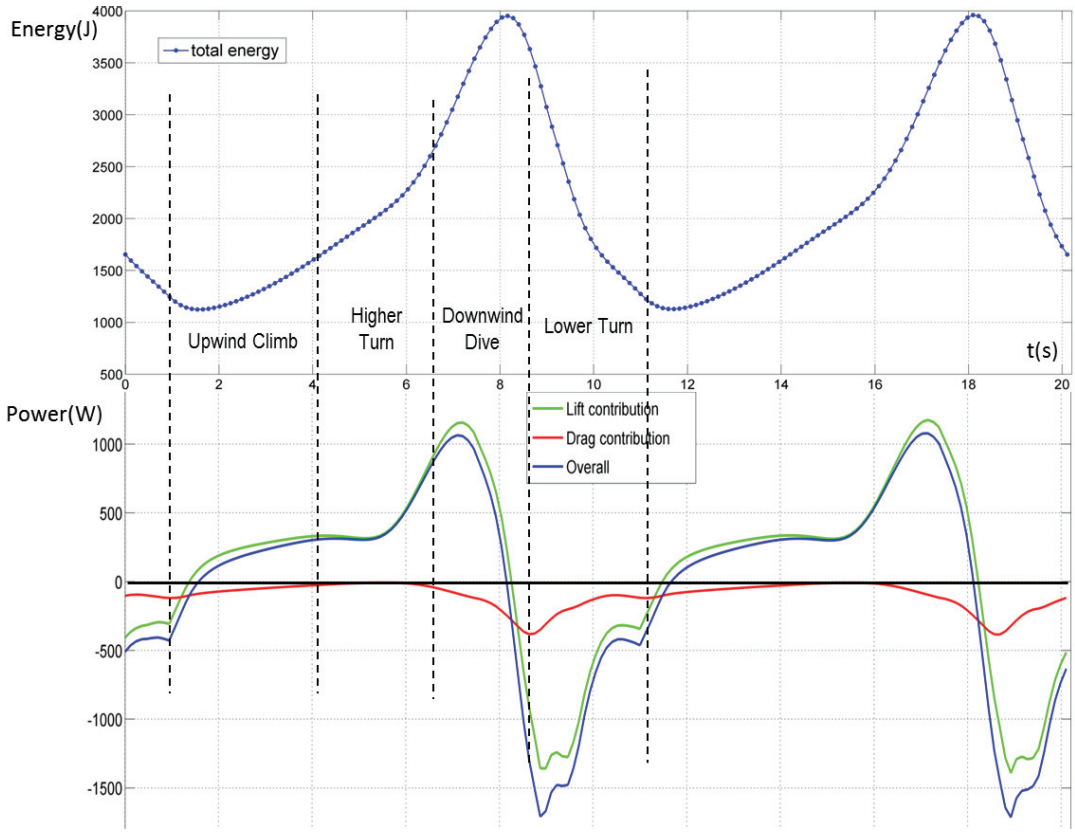

Figure 12. Variation in total energy with time and in the associated rate of energy with time

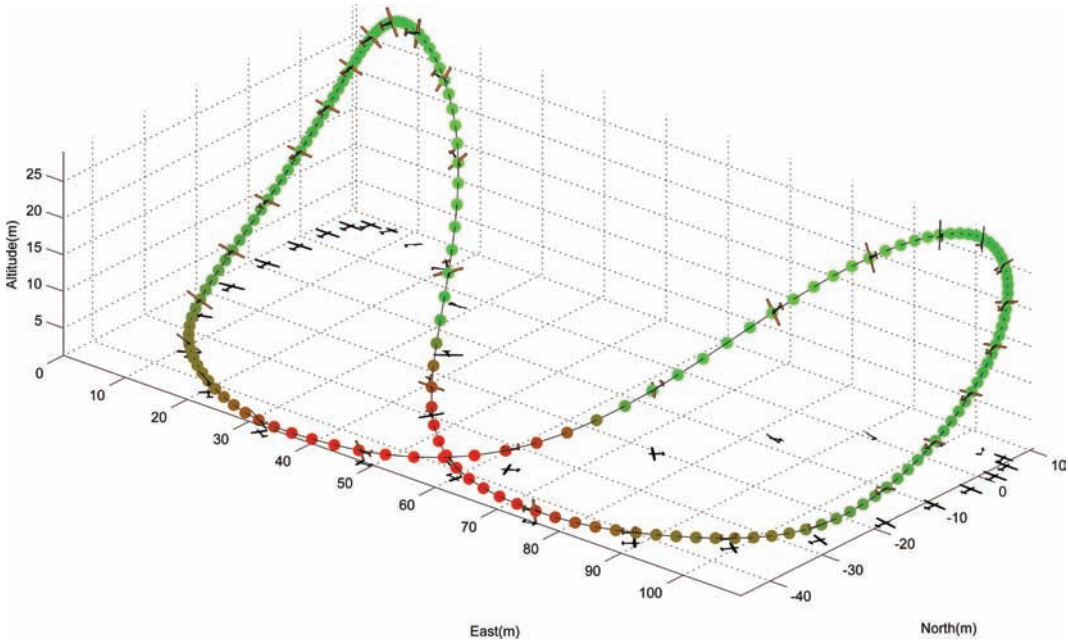

Figure 13. Overall energy-harvesting strategy. The energy neutral closed loop trajectory from Fig. 8 is colored following a red to green scale as a function of the local power input. Total energy is extracted at green-colored positions and is lost at red-colored positions.

5. CONCLUSION

This paper presents an analysis of energy-harvesting mechanisms characteristic to dynamic soaring flight. It was chosen to focus on the understanding of those principles rather than to provide extensive performance charts about dynamic soaring flight. The approach undertaken does not intend to substitute to performance-oriented studies but rather to complement those by shedding light on some in-depth aspect about the energy-extraction by dynamic soaring.

Equations of motion were specified to be part of a broader optimization problem, which was solved in the particular case of a closed trajectory. Results showed that it was not necessary to dispose of a wind gradient strong enough to sustain a steady airspeed during the upwind climb. A closed trajectory could be obtained for a reasonable set of parameters, with the exception perhaps of the wing tip clearance, which is only a 50 cm above the surface. It should be noted that minimum wind strength conditions found for the closed trajectory are much higher than results obtained by Deittert [14]. It can be explained by the maximum lift over drag ratio of more than 30 he gets for the vehicle and the fact that only the wing is modelled certainly accounts for this surprisingly high value. Besides, the existence of a solution to the problem of a closed trajectory validates the feasibility to fly by dynamic soaring regardless of the wind direction.

The contribution of aerodynamic forces to the variation in total energy was explicated and analysed with respect to geometrical parameters associated with successive manoeuvres. It was shown that the vehicle sees a gain in energy during the upwind climb, the upper turn as well as the downwind dive. It was shown that dynamic soaring not only consists in extracting energy, but in finding a compromise between gain and losses along the path. On that matter, it was shown that the lower turn has a significant adverse effect that could potentially be further optimized.

Finally, in order to reach an understanding about refined kinematics and energy-exchanges, it seems necessary to improve both the vehicle model and the wind model, in their accuracy. The point-mass model is simplistic to represent accurately the behaviour of a vehicle. Underlying degrees of freedom should be truly modelled rather than artificially constrained in order to guarantee the practicability of the flight path. For instance, the rate of roll would then no longer be apriori constrained, but governed by the equation that rules the rotational motion along the longitudinal axis. Furthermore, the biggest challenge seems to lay in the way to model the wind field, as a statistical model is probably too limited to accurately represent the first meters of an unsteady turbulent boundary layer above a rough surface. That also questions the choice of a point mass model, as the scale of turbulent-induced gradients is way

smaller than that of the mean wind profile. It calls for a refined vehicle model where the influence of span wise wind shear can be properly taken into account.

ACKNOWLEDGEMENTS

This PhD is financed by the French (DGA) under a dual agreement with DSTL to sponsor joint French/UK PhDs so as to develop research in key areas of mutual interest to France and the U.K.

REFERENCES

[1] Unmanned Aircraft Systems Road Map 2005-2030, U.S. Department of Defense, July 2005, p.51.

[2] Rosenberg, Z. *Liquid hydrogen extends fuel cell-powered UAV to 48h aloft*, Flight International, January 2013.

[3] Swider-Lyons, K.E., MacKrell, J. A., Rodgers, J., Page, G., Schuette, M., Stroman, R., *Hydrogen Fuel Cell Propulsion for Long Endurance Small UAVs*, AIAA Centennial of Naval Aviation Forum, AIAA 2011-6975, 21-22 September 2011.

[4] Pennycuick, C., *Modelling the Flying Bird* (Theoretical Ecology Series), 2008.

[5] Tickell, W., *Albatrosses*. Yale University Press, 2004.

[6] Lord Rayleigh, *The Soaring of Birds,* Nature, Vol. 27, No. 701, 5 April 1883, pp. 534-535.

[7] P.Idrac. *Etude expérimentale et analytique du vol sans battements des oiseaux voiliers des mers australes, de l'Albatross en particulier*. La Technique Aéronautique, Vol. 16, 1925, pp. 9-22.

[8] Wood, C. J., *The Flight of Albatrosses (a Computer Simulation*), Ibis, Vol 115, 1925, pp. 244-256.

[9] Jouventin, P., Weimerkirsch, H., *Satellite tracking of wandering albatrosses*, Nature, 1990, 343

[10] Birdlife International (2004). *Tracking Ocean Wanderer*, Cambridge UK: Birdlife International.

[11] *NASA Surface meteorology and solar energy: Methodology*, 12/16/04.

[12] Sachs, G., *Minimum shear wind strength required for dynamic soaring of albatrosses*, Ibis, Vol. 147, No. 1, 2004, pp. 1-10

[13] Zhao, Y., *Minimal fuel powered dynamic soaring of unmanned aerial vehicle utilizing wind gradients*, Optim. Control. Appl.Meth., Vol. 25, 2004, pp. 211-233.

[14] Deittert, M., Richards, A., Toomer, C., Pipe, A., *Engineless Unmanned Aerial Vehicle Propulsion by Dynamic Soaring*, Journal of Guidance, Control and Dynamics, Vol. 32, No.5, September-October 2009, pp. 1446-1454.

[15] Pennycuick, C., *Gust Soaring as the basis for the flight of albatrosses and petrels*, Avian Science, Vol. 2, No. 1, 2002, pp. 1-12

[16] Sachs, G., Traugott, J., Holzapfel, H., *Progress against the wind with Dynamic Soaring_Results from In-Flight Measurement of Albatrosses*, AIAA Guidance Navigation and Control Conference, AIAA 2011-6225, 2011.

[17] Richardson, P., *How do Albatross fly around the world without flapping their wings*?, Progress in Oceanography, Vol. 88, 2011, pp. 46-58.

[18] Bower, G. C., *Boundary Layer Dynamic Soaring for Autonomous Aircraft: Design and Validation*, Ph.D. Dissertation, Aeronautics and Astronautics Dept., Stanford, December 2011.

[19] Stull, R. B., *An introduction to boundary layer meteorology*, Kluwer Academic Publishers.

[20] Hull, D., *Conversion of Optimal Control Problem into Parameter Optimization Problems*, Journal of Guidance, Control and Dynamics, Vol. 20, No. 1, January-February 1997, pp. 57-60.

[21] Herman, A., Conway, B., *Direct Optimization Using Collocation Based on High-Order Gauss-Lobatto Quadrature rules*, Journal of Guidance, Control and Dynamics, Vol. 19, No. 3, May-June 1996, pp. 592-599.

[22] Gill, P., Murray, M., Saunders, M., *SNOPT: An SQP Algorithm for Large-Scale Constrained Optimization*, SIAM Rev. Vol. 47 , No. 1, pp. 99-131.